Available online at www.sciencedirect.com

SCIENCE DIRECT®

Journal of Molecular Catalysis A: Chemical 203 (2003) 193–202

JOURNAL OF MOLECULAR CATALYSIS A: CHEMICAL

www.elsevier.com/locate/molcata

Interaction of probe molecules with active sites on cobalt, copper and zinc-exchanged SAPO-18 solid acid catalysts

Chris Kladis, Suresh K. Bhargava*, Deepak B. Akolekar

Department of Applied Chemistry, RMIT University, GPO Box 2476V, Melbourne, Vic. 3001, Australia

Received 25 November 2002; accepted 29 March 2003

Abstract

Novel cobalt (Co), copper (Cu) and zinc (Zn) exchanged chabazite related SAPO-18 solid acid catalysts were prepared and characterised using techniques such as BET (nitrogen sorption), FTIR, ICP-OES, XPS and XRD. A detailed in situ FTIR investigation undertaken on the adsorption and disproportionation of NO and CO over Co-, Cu- and Zn-SAPO-18 molecular sieve catalysts indicated the formation of various NO/CO species or complexes with cationic Lewis acid and/or active metal sites. NO adsorption at room temperature leads to the formation of up to seven bands attributed to adsorbed nitrous oxide (N_2O), chemisorbed nitrogen dioxide (NO_2), nitrite (M-NO_2) (M, metal), mononitrosyl (M-NO) and dinitrosyl [M-$(NO)_2$] complexes. CO adsorption at room temperature leads to the formation of up to six bands attributed to physi-sorbed carbon dioxide (CO_2), cationic Lewis acid carbonyl moieties (L-CO) and transition metal carbonyl complexes (M-CO). The concentration and distribution of NO/CO species varies with pressure, reaction temperature and evacuation.
© 2003 Elsevier Science B.V. All rights reserved.

Keywords: FTIR spectroscopy; SCR; Nitric oxide; Carbon monoxide; Co-SAPO-18; Cu-SAPO-18; Zn-SAPO-18; Lewis acid sites; Active metal sites

1. Introduction

As previously reported by Iwamoto et al., Cu-ZSM-5 was found to be active for the decomposition of NO_x [1–4]. Its potential application in the selective catalytic reduction (SCR) of NO_x from oxygen rich combustion processes was impaired by the reversible or irreversible suppression of catalytic activity by water vapour and SO_2. Other catalysts such as Cu-exchanged SAPO-*n* molecular sieves ($n = 5$, 11, 34) and zeolites (□, USY and ZSM-5) are known to be active for the SCR of NO with hydrocarbons in the presence of oxygen [5–8]. Crystalline silicoaluminophosphates (SAPO-*n*) are a new class of microporous inorganic solids with many applications as catalysts, ion exchangers and molecular sieves [9–12].

Crystalline microporous $AlPO_4$ composed of corner sharing tetrahedral AlO_4 and PO_4 units are a new generation of molecular sieves with effective properties similar to zeolitic materials. Substitution of heteroatoms into the $AlPO_4$ framework produces solid acids of variable acid strength. $AlPO_4$-18 molecular sieve is a crystallographically novel but chabazite related material like SAPO-34. The main structural difference between $AlPO_4$-18 and SAPO-34 lies in the orientation of the double hexagonal prisms from which both are built. In $AlPO_4$-18, alternate layers of hexagonal prisms parallel to the *ab*-plane are related by a

* Corresponding author. Tel.: +61-3-9925-3365; fax: +61-3-9639-1321.
E-mail addresses: ckladis@yahoo.com.au (C. Kladis), suresh.bhargava@rmit.edu.au (S.K. Bhargava), E04781@ems.rmit.edu.au (D.B. Akolekar).

1381-1169/03/$ – see front matter © 2003 Elsevier Science B.V. All rights reserved.
doi:10.1016/S1381-1169(03)00262-0

c-axis glide and thereby possess different orientations. This causes the supercage formed between hexagonal prisms to have a pear-like shape. Due to structural similarities, SAPO-18 is expected to exhibit similar Brønsted acidity to SAPO-34 [9–12].

Cu-SAPO-34 catalyst sustains the high catalytic activity for NO SCR for more than 60 h at 473 K in an atmosphere containing 15% water vapour and remains unaffected up to 1073 K. The behaviour of Cu ions in SAPO-34 follows a redox mechanism between monovalent and divalent states [5–8]. Transition metal modified microporous materials display unique selectivity in catalysis, adsorption science and ion-exchange, as well as exhibiting significant catalytic activity towards the decomposition of air pollutants (NO_x, CO_x and SO_x). The interaction of molecular species with active metal sites is usually investigated by FTIR using nitric oxide (NO) and carbon monoxide (CO) probe molecules. In the present paper, the adsorption-interaction of typical probe molecules with active metal species on modified silicoaluminophosphate solid acid catalysts was investigated. Such NO/CO adsorption experiments were undertaken to elucidate the nature of active metal sites under varying experimental conditions.

2. Experimental

2.1. Catalyst preparation

Co-, Cu- and Zn-exchanged SAPO-18 were prepared by a liquid ion-exchange method. Calcined SAPO-18 was ion-exchanged with a 0.010 M transition metal nitrate solution. The suspension was stirred at 343 K for 2 h and the solid collected by filtration, washed with distilled water and dried. The entire ion-exchange process was repeated thrice. After the third ion-exchange, the material was calcined in air at 773 K for 5 h. SAPO-18 was obtained by calcination of as-synthesised SAPO-18. As-synthesised SAPO-18 was prepared by hydrothermal crystallisation of gel (molar composition: 1.6 $C_8H_{19}N$; 1.0 Al_2O_3; 0.4 SiO_2; 0.9 P_2O_5; 50 H_2O) in a Teflon-lined stainless steel autoclave at 443 K for 8 days [13,14]. The crystallisation product was filtered, thoroughly washed and dried in air at 343 K. The organic template was removed by calcination in a muffle furnace at 773 K for 16 h. The chemicals used for synthesis were catapal B (68% boehmite, Vista), *o*-phosphoric acid (85%, Merck), aerosil (99%, Degussa) and *N*,*N*-diisopropylethylamine (99%, Aldrich).

2.2. Catalyst characterisation

Bulk chemical composition of transition metal exchanged SAPO-18 was determined by ICP-OES using a Perkin-Elmer Optima 3300 DV instrument. Surface area and micropore volume of the materials was obtained by the N_2-dynamic adsorption/desorption technique using a Micromeritics ASAP2000 instrument. X-ray powder diffraction patterns were obtained with a Philips PA2000 diffractometer using a Ni-β filtered Cu Kα (1.5406 Å) X-ray source. XPS surface analysis was conducted for determining the surface concentrations and binding energies of Si 2p, Al 2p, P 2p, O 1s, Co 2p, Cu 2p and Zn 2p using a Fisons Microlab 310F instrument operating in the constant pass energy mode. All spectra were referenced to C 1s (285 eV).

2.3. FTIR measurements

FTIR studies were performed on self-supported wafers (ca. 20 mg). A self-supported wafer was fixed to a sample holder of a Pyrex high temperature FTIR cell with NaCl windows. All samples were first activated under vacuum ($<10^{-4}$ Torr) at 573 K for 16 h. A high purity mixture of nitrogen (95%) and nitric oxide (5%) and carbon monoxide (99.95%) supplied by Linde, Australia were used as the NO or CO source. FTIR spectra were obtained using Perkin-Elmer System 2000 FTIR spectrometer equipped with deuterated triglycine sulphate (DTGS) and mercury cadmium telluride (MCT) detectors. The spectra of dehydrated catalyst samples were used as a background from which the adsorbed probe molecule spectra were subtracted. All spectra were collected at room temperature and at different gas pressures depending upon experimental conditions. FTIR spectra were obtained in the mid-infrared region, over the range 4000–1400 cm^{-1}, with 64 co-added scans at 2 cm^{-1} spectral resolutions. All spectra were recorded in the transmission mode, smoothed and baseline corrected.

3. Results and discussion

Highly crystalline SAPO-18 with a molar composition of 54.5 Al, 34.7 P and 10.8 Si was utilised for the preparation of Co-, Cu- and Zn-exchanged SAPO-18 molecular sieve catalysts. Characterisation of transition metal exchanged SAPO-18 materials by BET, ICP-OES and XRD confirmed the high purity and crystallinity. The characteristics of transition metal exchanged SAPO-18 materials are presented in Table 1. The XRD shows strong reflections at 9.1 and 5.1° 2θ, characteristic for as-synthesised AEI materials. The competing phase of AEI materials is AFI when $P_2O_5/Al_2O_3 > 1.2$ or $R/P_2O_5 < 1.2$ [13,14]. The XRD patterns of AEI materials are very sensitive to water molecules present in the channels of the structure.

Nitrogen sorption data (BET) for transition metal exchanged SAPO-18 materials is presented in Table 1. Nitrogen sorption is high for SAPO-18 (653 m^2/g surface area and 0.25 cm^3/g micropore volume) but decreases after ion-exchange with transition metals, indicating a high decrease in porosity [15]. Ion-exchange with transition metals results in micropore blockage, which leads to a reduction or distortion in the volume and shape of SAPO-18 micropores [16]. The low transition metal loading, and relative small decrease in surface area and micropore volume indicate a low concentration of Co, Cu and Zn active sites evenly spread throughout the SAPO-18 molecular sieve.

Bulk chemical and XPS surface analysis (Tables 1 and 2) for transition metal exchanged SAPO-18 catalysts indicate that the concentrations of silicon, aluminium and phosphorous are higher in the bulk rather than on the surface. The lower surface transition metal to aluminium and transition metal silicon ratios indicate a higher concentration of transition metal ions in the bulk rather than on the surface of SAPO-18 (Table 2). This is confirmed by the BET nitrogen sorption results, which show a small decrease in surface area and micropore volume after exchange with transition metal ions. XPS analysis revealed the existence of Co metal ions in the +2 and +3 oxidation states while Cu and Zn metal ions existed predominantly in the +2 oxidation state. The binding energies of the other elements (O 1s, Si 2p, Al 2p, P 2p) are close to those for tetrahedrally coordinated elements in metal substituted aluminophosphates [17] and low silica zeolites [18]. In situ FTIR study revealed the presence of the four types of hydroxyl groups on pure dehydrated SAPO-18 at 3740, 3675, 3615 and 3520 cm^{-1} ascribed to the fundamental stretching vibrations of terminal SiOH and/or surface AlOH and POH, undisturbed bridging hydroxyl (SiOHAl) groups with Brønsted acidic character and hydroxyl groups attached to multivalent cations, respectively. With transition metal exchanged SAPO-18, a slight decrease in band intensity of all OH groups was observed.

Table 2
Comparison of bulk and surface chemical composition for the transition metal exchanged SAPO-18 solid acid catalysts

Catalyst	Surface			Bulk		
	Si/Al	Si/P	P/Al	Si/Al	Si/P	P/Al
SAPO-18	0.48	0.99	0.49	0.20	0.31	0.64
Co-SAPO-18	0.24	0.81	0.29	0.19	0.27	0.70
Cu-SAPO-18	0.15	0.48	0.32	0.19	0.29	0.65
Zn-SAPO-18	0.15	0.44	0.33	0.19	0.27	0.69

3.1. Adsorption of NO on transition metal exchanged SAPO-18

Nitric oxide adsorption on heterogeneous catalysts is a widely used technique in the investigation of the nature and properties of adsorption sites present on the catalyst surface. FTIR spectroscopy is a technique commonly utilised to investigate NO adsorption on

Table 1
Comparison of physical and chemical properties for the transition metal exchanged SAPO-18 solid acid catalysts

Catalyst sample	Product composition (mol%)	Surface area (m^2/g)	Micropore volume (cm^3/g)
SAPO-18	Si, 10.8; Al, 54.5; P, 34.7	653	0.25
Co-SAPO-18	Co, 0.5; Si, 10.0; Al, 52.7; P, 36.8	460	0.17
Cu-SAPO-18	Cu, 2.8; Si, 10.0; Al, 52.7; P, 34.5	480	0.18
Zn-SAPO-18	Zn, 1.7; Si, 9.9; Al, 52.3; P, 36.1	503	0.19

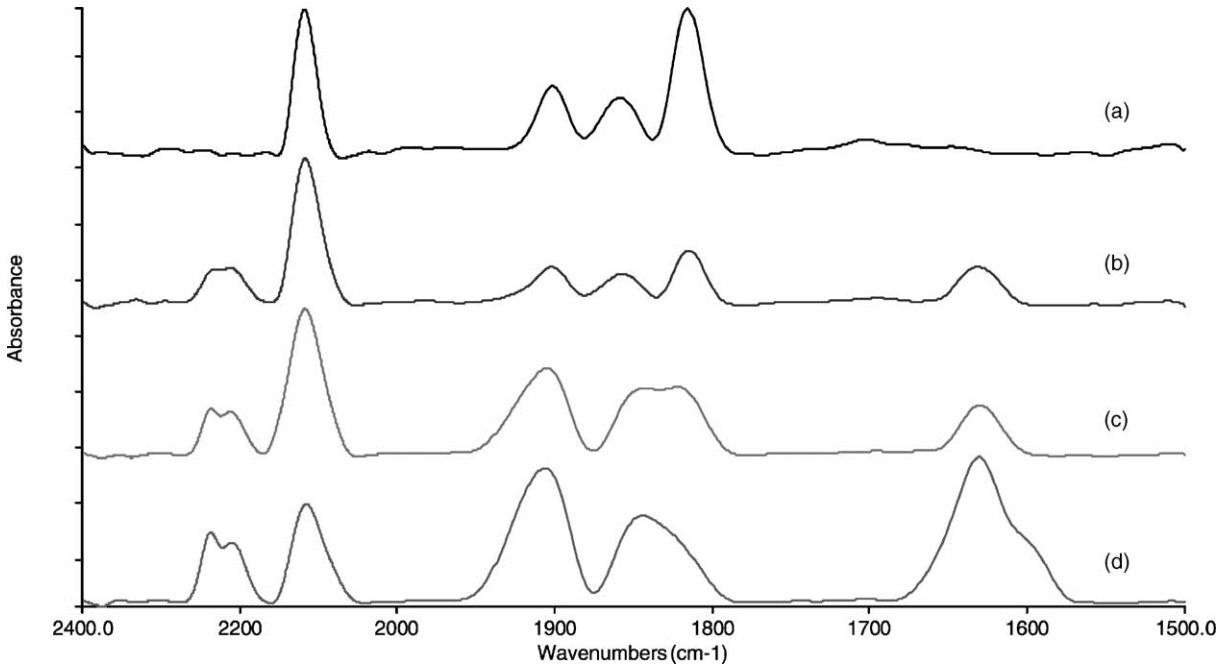

Fig. 1. FTIR spectra of NO adsorbed at various pressures over the dehydrated Co-SAPO-18 catalyst: (a) 22 Torr, (b) 61 Torr, (c) 72 Torr and (d) 103 Torr.

catalysts. The infrared frequencies and changes in the frequencies of the stretching vibrations of the adsorbed probe molecule give information about the adsorption sites (e.g. types of sites, the oxidation state of the metal and the state and localisation of the cations). The interaction between NO and transition metal exchanged SAPO-18 is depicted in Figs. 1–3. After dehydration of Co-, Cu- and Zn-exchanged SAPO-18 in vacuo at 573 K for 16 h, exposure to NO resulted in up to seven bands attributed to the formation of nitrous oxide (N_2O), chemisorbed nitrogen dioxide (NO_2), nitrite (M-NO_2) (M, metal), mononitrosyl (M-NO) and dinitrosyl [M-$(NO)_2$] complexes. The assignment of infrared bands is consistent with the literature data [19–28].

FTIR spectra of NO adsorption over activated Co-SAPO-18 at 298 K are shown in Fig. 1. Exposure to 22 Torr NO (Fig. 1a) produced four bands attributed to the formation of chemisorbed NO_2 (2120 cm^{-1}), Co^{III}-NO (1900 cm^{-1}), Co^{II}-$(NO)_2$ (1845 cm^{-1}) and Co^{II}-NO (1810 cm^{-1}). Adsorption of NO at 61 Torr (Fig. 1b) leads to an increase in concentration of chemisorbed nitrogen dioxide and the appearance of an infrared band attributed to a cobalt-nitrite moiety (Co^{III}-NO_2). The intensity of the Co^{II}-NO band decreased with an increase in NO pressure. NO adsorption at 72 and 103 Torr (Fig. 1c and d) leads to a further increase in NO surface coverage and hence intensities of the infrared bands at 2240, 1910 and 1845 cm^{-1}. The presence of bands attributed to adsorbed N_2O and Co^{III}-NO_2 indicate oxidation of Co^{II} active sites to Co^{III}. Formation of Co^{III} occurs when the Co^{II}-$(NO)_2$ complex is oxidised by NO and forms an unstable Co^{III} complex with N_2O and O^- adsorbed species. Further reaction with NO sees the conversion of the unstable N_2O and O^- intermediates to Co^{III}-NO_2. Evacuation of the NO gas phase (10^{-4} Torr) at room temperature for 30 min leads to desorption of the Co-NO species. The chemisorbed nitrite and cobalt-nitrite species remained relatively unaffected by evacuation.

In situ FTIR spectra of NO adsorption on the dehydrated Cu- and Zn-SAPO-18 molecular sieves at 298 K and increasing gas pressures are shown in Figs. 2 and 3. Adsorption of NO at 22 Torr (Figs. 2a and 3a) leads to the appearance of up to two strong and two

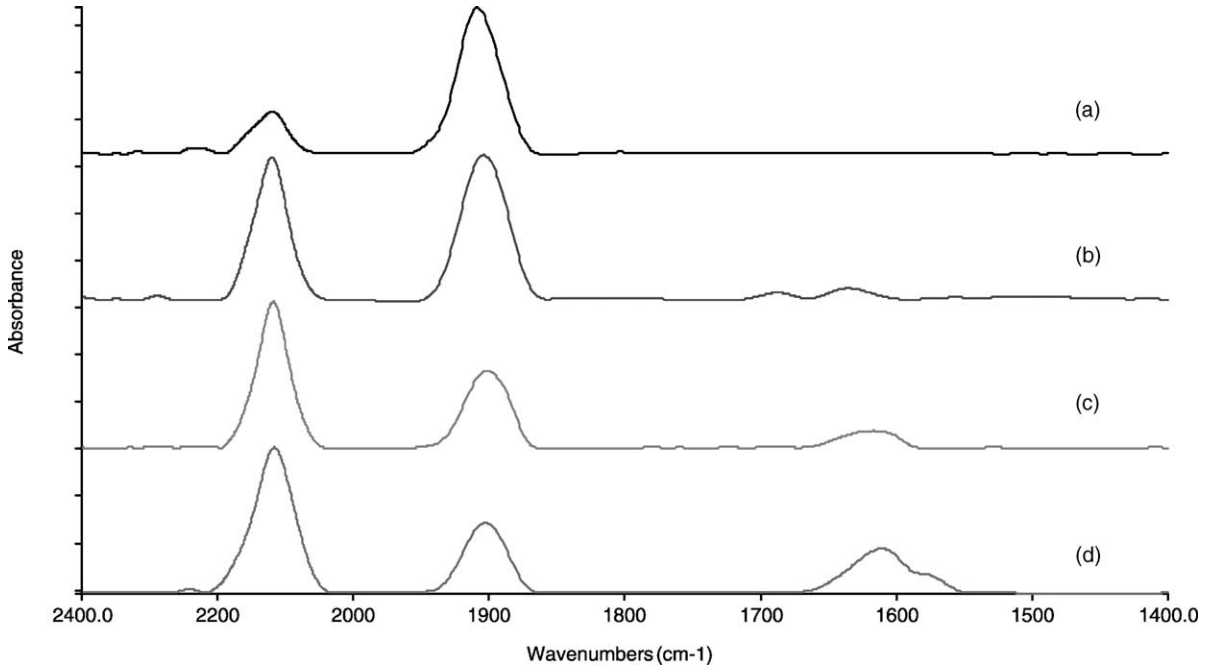

Fig. 2. FTIR spectra of NO adsorbed at various pressures over the dehydrated Cu-SAPO-18 catalyst: (a) 22 Torr, (b) 61 Torr, (c) 72 Torr and (d) 103 Torr.

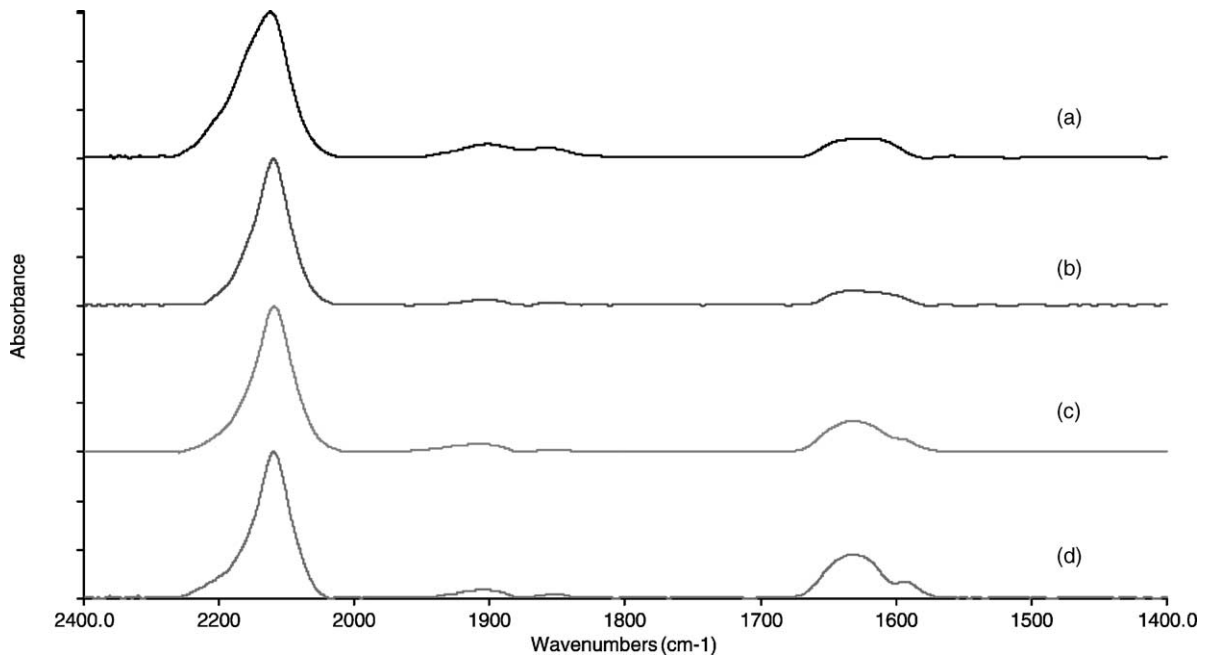

Fig. 3. FTIR spectra of NO adsorbed at various pressures over the dehydrated Zn-SAPO-18 catalyst: (a) 22 Torr, (b) 61 Torr, (c) 72 Torr and (d) 103 Torr.

weak vibrations at 2120, 1910, 1845 and 1630 cm^{-1}, attributed to chemisorbed NO_2, M^{II}-NO, M^{II}-$(NO)_2$ and M^{II}-NO_2 complexes, respectively. No bands attributed to Cu^{I}-NO are observed as XPS indicates the presence of predominantly Cu^{2+} active metal sites. NO adsorption at 61, 72 and 103 Torr (Figs. 2b–d and 3b–d) leads to an increase in intensity of the chemisorbed NO_2 band, the appearance of a band attributed to M^{II}-NO_2 and a decrease in intensity of the bands attributed to M^{II}-NO and M^{II}-$(NO)_2$. The Cu^{II} and Zn^{II} nitrite complexes react with NO to produce unstable Cu^{II} and Zn^{II} intermediates with N_2O and O^- adsorbed species. Further reaction with nitric oxide leads to conversion of the unstable N_2O and O^- intermediates into a M^{II}-NO_2 complex. Evacuation of the NO gas phase (10^{-4} Torr) for 30 min at room temperature leads to desorption of most of the adsorbed species. The band attributed to M^{II}-NO_2 intensifies after evacuation of the FTIR cell.

The adsorption of NO over transition metal exchanged SAPO-18 resulted in the formation of M-NO, M-$(NO)_2$, M-NO_2, adsorbed N_2O and chemisorbed NO_2 species. The reaction mechanism by proposed by Giamello et al. [19] and Spoto et al. [20] for the adsorption and disproportionation of NO over Cu-ZSM-5 are in good agreement with the results presented in this paper. Interaction of NO with Co-SAPO-18 resulted in the formation a mononitrosyl species (Co^{II}-NO) with a band appearing at 1810 cm^{-1}. Unlike copper exchanged ZSM-5 and SAPO-34, this band was not observed on the Cu-SAPO-18 catalyst, and it is believed that most of the Cu^{I} active metal sites had been already oxidised to the Cu^{II} oxidation state.

After initial formation of M-NO, a second NO molecule adsorbs onto M-NO at higher equilibrium pressure to form a dinitrosyl moiety with stretching vibrations at 1845 cm^{-1} (asymmetric) and 1735 cm^{-1} (symmetric). Giamello et al. [19] and Spoto et al. [20] found that adsorption of a second NO molecule is usually followed by oxidation of the active metal catalyst. Both researchers agree that oxidation occurs at the site of the dinitrosyl complex. This involves bonding of two N atoms to form an unstable intermediate. Excess NO can displace the N_2O species to give an infrared band at 2240 cm^{-1}, which is characteristic of adsorbed N_2O. The reactive O^- site reacts with another NO molecule to produce a M-NO_2 complex with a vibrational band at 1630 cm^{-1}. To regenerate the active metal sites, surface oxygen has to be removed by desorption or reduction.

3.2. Adsorption of CO on transition metal exchanged SAPO-18

Carbon monoxide chemisorption on activated microporous materials provides information about the oxidation and coordination state of charge balancing cations. This technique is widely employed for analysis of active sites on ion-exchanged molecular sieves because of its ability to act as a weak σ-donor and π-acceptor, its sensitivity towards electrostatic fields surrounding metal cations and its ability to interact with Lewis acid sites. Modified SAPO-18 samples were used to investigate the interaction of CO using the in situ FTIR technique. The interaction between CO and transition metal exchanged SAPO-18 is depicted in Figs. 4–6. After dehydration of Co-, Cu- and Zn-exchanged SAPO-18 in vacuo at 573 K for 16 h, exposure to CO produced vibrational spectra with up to six bands attributed to the formation of physi-sorbed carbon dioxide, cationic Lewis acid carbonyl moieties (L-CO) and transition metal carbonyl complexes (M-CO). These infrared bands are consistent with the reported literature [28–36].

CO adsorption on activated Co- and Zn-SAPO-18 solid acid catalyst at 298 K and increasing equilibrium pressures is depicted in Figs. 4 and 5. The FTIR spectra of CO adsorption at 22 Torr produced two strong and two weak vibrations at 2350, 2170, 2120 and 2060 (sh) cm^{-1} (Figs. 4a and 5a). Vibrational spectra at 61, 72 and 103 Torr CO are shown in Figs. 4b–d and 5b–d. At these higher CO gas pressures, the four observed infrared bands remain relatively unchanged. A weak band at 2350 cm^{-1} developed during CO adsorption on Co- and Zn-SAPO-18 is attributed to the ν_3 vibration of adsorbed CO_2, linearly bound to the cation by ion-induced dipole interactions [27,29,33,35]. The band at 2350 cm^{-1} is therefore a good indicator of CO_2 formation during the adsorption of CO over transition metal exchanged SAPO-18 solid acid catalysts. The infrared band at 2170 cm^{-1} is assigned to CO adsorbed by the carbon on to cationic Lewis acid sites while the band at 2120 cm^{-1} is assigned to CO adsorbed on to SAPO-18 cationic Lewis acid sites by the oxygen atom [30–33,35]. A weak shoulder

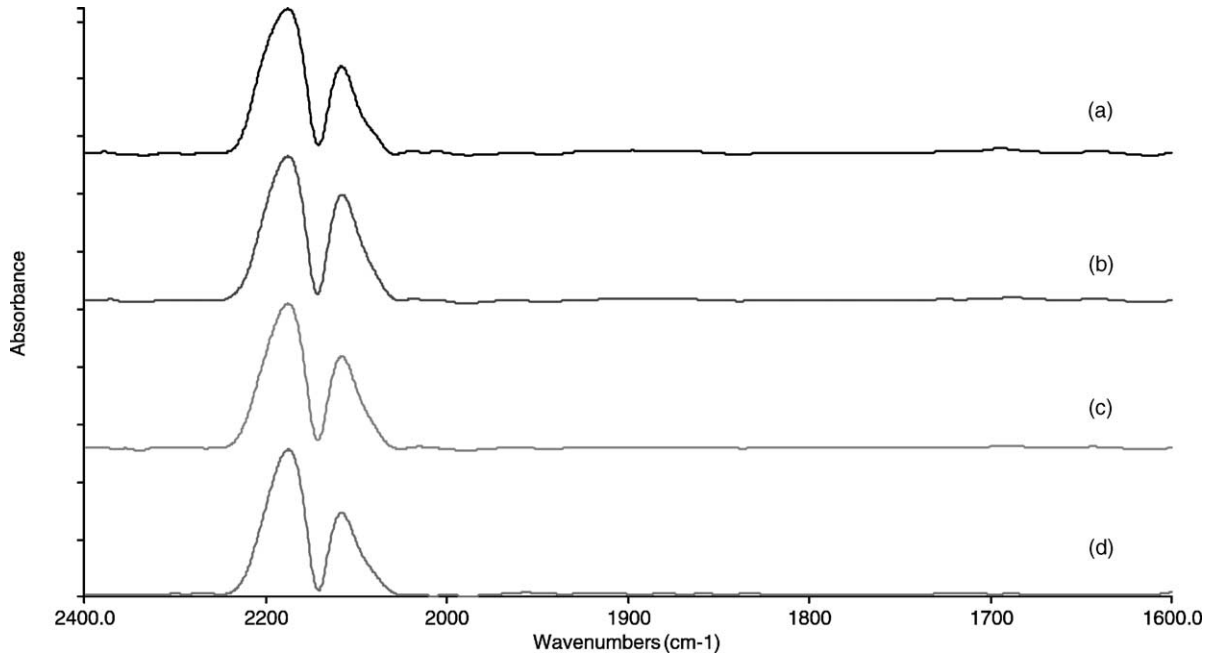

Fig. 4. FTIR spectra of CO adsorbed at various pressures over the dehydrated Co-SAPO-18 catalyst: (a) 22 Torr, (b) 61 Torr, (c) 72 Torr and (d) 103 Torr.

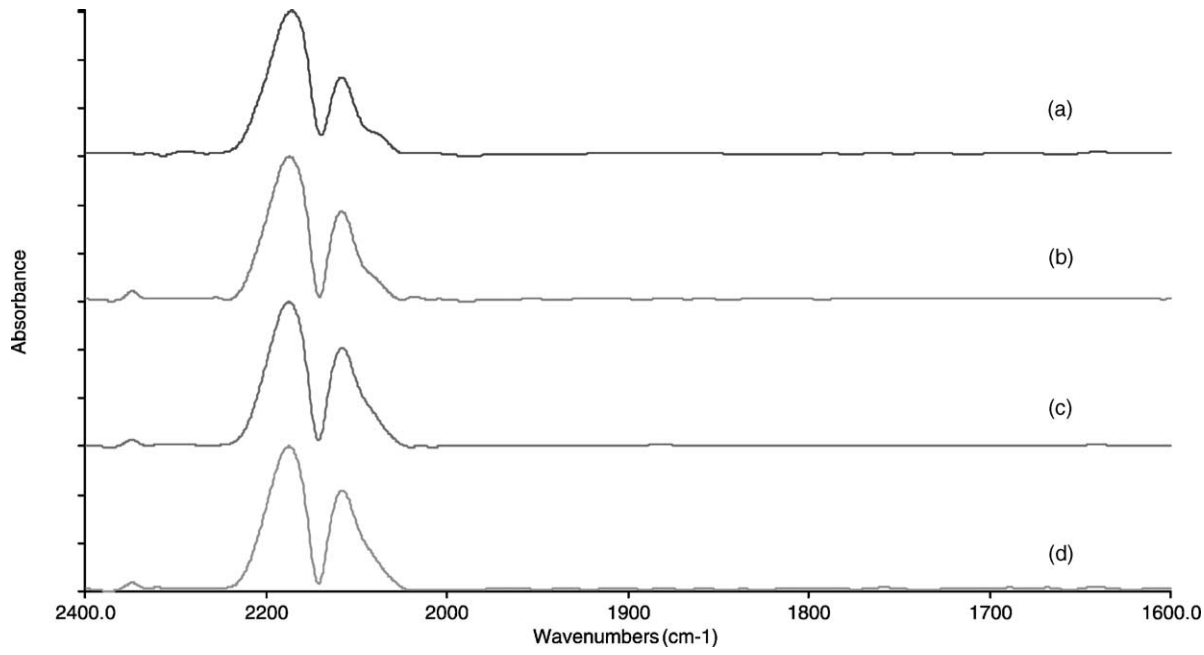

Fig. 5. FTIR spectra of CO adsorbed at various pressures over the dehydrated Zn-SAPO-18 catalyst: (a) 22 Torr, (b) 61 Torr, (c) 72 Torr and (d) 103 Torr.

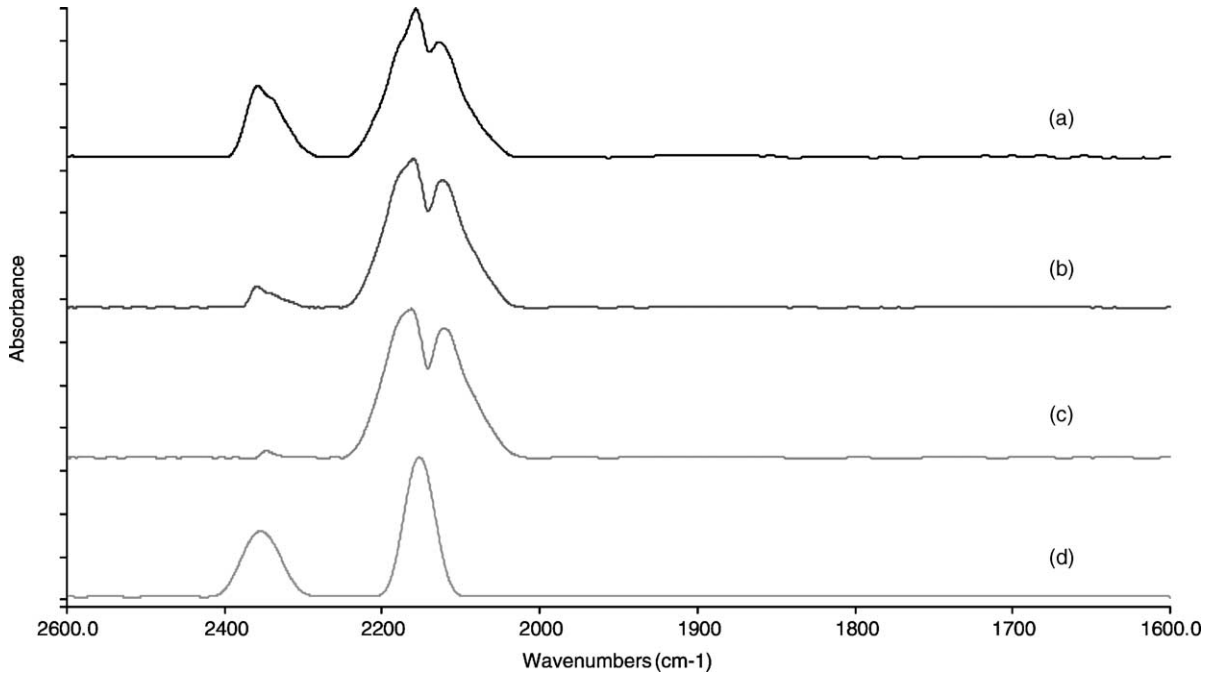

Fig. 6. FTIR spectra of CO adsorbed at various pressures over the dehydrated Cu-SAPO-18 catalyst: (a) 22 Torr, (b) 61 Torr, (c) 7 Torr and (d) evacuation at room temperature for 30 min.

band observed 2060 cm^{-1} is characteristic of terminal stretching CO vibrations present in metal-carbonyl species. Evacuation of the high temperature infrared cell (10^{-4} Torr) at 298 K for 30 min resulted in the disappearance of all the observed infrared active species.

Fig. 6 displays the FTIR spectra of vacuum-dehydrated Cu-SAPO-18 after exposure to CO at 298 K. Adsorption of 22 Torr CO leads to the appearance of five infrared bands at 2350, 2195, 2170, 2155 and 2120 cm^{-1} (Fig. 6a). Infrared spectra of CO adsorption at 61 and 72 Torr are shown in Fig. 6b and c. At these equilibrium pressures, the two bands at 2170 and 2120 cm^{-1} increased in intensity indicating a greater surface coverage while the intensity of a band at 2350 cm^{-1} decreased. The band at 2350 cm^{-1} developed during adsorption of CO on Cu-SAPO-18 is attributed to the ν_3 vibration of adsorbed CO_2, linearly bound to Cu by ion-induced dipole interactions [27,29,33,35]. The infrared band at 2170 cm^{-1} is assigned to CO adsorbed by the carbon on to SAPO-18 cationic Lewis acid sites, while the band at 2120 cm^{-1} is assigned to CO adsorbed on to SAPO-18 cationic Lewis acid sites by the oxygen atom [30–33,35]. A weak fourth vibration at 2195 cm^{-1} (sh), disappearing after evacuation is assigned to Cu^{II}-CO species [34–36]. Evacuation of the FTIR cell (10^{-4} Torr) at 298 K for 30 min leads to desorption of the moieties at 2170 and 2120 cm^{-1}, indicating the presence of weakly adsorbed species on the Cu-SAPO-18 framework, while the remaining band at 2350 cm^{-1} indicates a continued presence of framework CO_2. Deconvolution of the spectrum indicates the presence of a fifth infrared band at 2155 cm^{-1}. The band is resistant towards evacuation and indicates chemisorption of CO molecules on Cu^{I} sites similar to those observed on Cu-ZSM-5 and Cu-SAPO-34 [8,34–36].

The main products formed from the interaction of CO with transition metal exchanged SAPO-18 catalysts are weakly adsorbed carbonyl species (CO) with vibrations at 2170 and 2120 cm^{-1}. The infrared band at 2170 cm^{-1} is assigned to CO adsorbed by the carbon on to SAPO-18 tri-coordinated aluminium atoms (Lewis acid sites) while the band at 2120 cm^{-1} can be assigned to CO adsorbed by the oxygen on to SAPO-18 Lewis acid sites. As these two C–O bands disappear from the spectrum upon evacuation of the

infrared cell at room temperature, it is apparent that the CO molecules are held by dipole–dipole type weak forces and are localised within the cavities of the SAPO-18 molecular sieve [30–33,35]. A band appearing at a frequency near the asymmetric stretch vibration of gas-phase CO_2 (2350 cm^{-1}) appears on the Cu- and Zn-SAPO-18 catalysts. It is attributed to the ν_3 vibration of adsorbed CO_2 on the catalyst surface [27,29,33,35]. Three infrared bands attributed to stretching vibrations of terminal metal–carbonyl bonds appear in transition metal exchanged SAPO-18 [8,32–36]. The first two bands, observed as weak shoulder vibrations at frequencies of 2195 and 2060 cm^{-1} are attributed to linear Cu^{II}-CO species while the third band at 2155 cm^{-1}, observed only on Cu-SAPO-18 is attributed to a chemisorbed Cu^{I}-CO moiety similar to that observed on Cu-ZSM-5 and Cu-SAPO-34.

4. Conclusions

The adsorption of nitric oxide on Co-, Cu- and Zn-SAPO-18 solid acid catalysts resulted in the formation of adsorbed N_2O, chemisorbed NO_2, M-NO, M-$(NO)_2$ and M-NO_2 species. Nitric oxide pressure affects the concentration and distribution of the NO complexes formed. The concentration of Co^{II}-NO decreased while those of adsorbed N_2O, Co^{III}-NO, Co^{II}-$(NO)_2$ and Co^{III}-NO_2 increased indicating, conversion of nitrosyl species to nitrite and oxidation of the Co^{II} active sites to Co^{III}. A similar pattern is observed with the Cu- and Zn-SAPO-18 molecular sieves, where metal-nitrosyl species decrease with the appearance of metal-nitrite moieties. Chemisorbed nitrite is present on the catalyst and is not affected by changes in NO equilibrium pressure. Evacuation of the FTIR cell at room temperature leads to desorption of the metal-nitrosyl species leaving metal-nitrite complexes as the only surface stable species at room temperature. Adsorption of carbon monoxide on Co-, Cu- and Zn-SAPO-18 solid acid catalysts resulted in the formation of carbonyls predominantly associated with cationic Lewis acid sites. Carbonyls linearly bound to active transition metal sites were also observed as weak shoulder bands, not resistant to evacuation under ambient conditions. Deconvolution of the Cu-SAPO-18 spectrum indicates the presence of a band resistant towards evacuation and associated with chemisorbed of CO molecules on Cu^{I} sites similar to that observed on Cu-ZSM-5 and Cu-SAPO-34. A third vibration developed during adsorption of CO on Cu- and Zn-SAPO-18. This band was attributed to the ν_3 vibration of adsorbed CO_2, linearly bound to Cu^{II} and Zn^{II} active sites by ion-induced dipole interactions.

References

[1] M. Iwamoto, Future Opportunities in Catalytic and Separation Technology, Elsevier, Amsterdam, 1990.
[2] M. Iwamoto, H. Yahiro, K. Tanda, N. Mizuno, Y. Mine, S. Kagawa, J. Phys. Chem. 95 (1991) 3727.
[3] M. Iwamoto, H. Hamada, Catal. Today 10 (1991) 57.
[4] M. Iwamoto, Stud. Surf. Sci. Catal. 84 (1994) 1395.
[5] T. Ishihara, M. Kagawa, F. Hadama, Y. Takita, Stud. Surf. Sci. Catal. 84 (1994) 1493.
[6] T. Ishihara, M. Kagawa, F. Hadama, Y. Takita, J. Catal. 169 (1997) 93.
[7] H. Nishiguchi, S. Kimura, T. Ishihara, Y. Takita, Res. Chem. Intermed. 24 (1998) 391.
[8] D.B. Akolekar, S.K. Bhargava, Stud. Surf. Sci. Catal. 105 (1998) 755.
[9] S.T. Wilson, B.M. Lok, C.A. Messina, T.R. Cannan, E.M. Flanigen, J. Am. Chem. Soc. 104 (1982) 1146.
[10] B.M. Lok, C.A. Messina, R.L. Patton, R.T. Gajek, T.R. Cannan, E.M. Flanigen, J. Am. Chem. Soc. 106 (1984) 6092.
[11] A. Dyer, An Introduction to Zeolite Molecular Sieves, Wiley, New York, 1988.
[12] D.B. Akolekar, Appl. Catal. A: Gen. 171 (1998) 261.
[13] A. Simmen, L. McCusker, C. Baerlocher, W. Meier, Zeolites 11 (1991) 654.
[14] J. Chen, P.A. Wright, J.M. Thomas, S. Natarajan, L. Marchese, S.M. Bradley, G. Sankar, C.R. Catlow, P.L. Gai-Boyes, R.P. Townsend, C.M. Lok, J. Phys. Chem. 98 (1994) 10216.
[15] D.B. Akolekar, S.K. Bhargava, J. Gorman, P. Paterson, Colloids Surf. A: Physiochem. Eng. Asp. 146 (1999) 375.
[16] D.W. Breck, Zeolite Molecular Sieves: Structure Chemistry and Use, Wiley, New York, 1974.
[17] D.B. Akolekar, J. Catal. 143 (1993) 227.
[18] M. Huang, A. Adnot, S. Kaliaguine, J. Catal. 137 (1992) 322.
[19] E. Giamello, D. Murphy, G. Magnacca, C. Morterra, Y. Shioya, T. Nomura, M. Anpo, J. Catal. 136 (1992) 510.
[20] G. Spoto, A. Zecchina, S. Bordiga, G. Richiardi, G. Mata, Appl. Catal. B: Environ. 3 (1994) 151.
[21] T. Cheung, S.K. Bhargava, M. Hobday, K. Foger, J. Catal. 158 (1996) 301.
[22] D.B. Akolekar, S.K. Bhargava, K. Foger, J. Chem. Soc., Faraday Trans. 94 (1998) 155.
[23] K. Hadjiivanov, Catal. Rev.-Sci. Eng. 42 (2000) 71.
[24] C. Kladis, S.K. Bhargava, K. Foger, D.B. Akolekar, Catal. Today 63 (2000) 297.

[25] C. Kladis, S.K. Bhargava, K. Foger, D.B. Akolekar, J. Mol. Catal. A: Chem. 171 (2001) 243.
[26] C. Kladis, S.K. Bhargava, K. Foger, D.B. Akolekar, J. Mol. Catal. A: Chem. 175 (2001) 241.
[27] D.B. Akolekar, S.K. Bhargava, Appl. Catal. A: Gen. 207 (2001) 355.
[28] R. Keiski, M. Harkonen, A. Lahti, T. Maunula, A. Savimaki, T. Slotte, Stud. Surf. Sci. Catal. 96 (1995) 85.
[29] J. Ward, H. Habgood, J. Phys. Chem. 70 (1966) 1178.
[30] C. Angell, P. Schaffer, J. Phys. Chem. 70 (1966) 1413.
[31] A. Zecchina, E. Escalona Platero, C. Otero Arean, J. Catal. 107 (1987) 244.
[32] A. Zecchina, S. Bordiga, D. Scarano, G. Petrini, G. Leofanti, M. Padovan, C. Otero Arean, J. Chem. Soc., Faraday Trans. 88 (1992) 2959.
[33] V.S. Kamble, N.M. Gupta, V.B. Kartha, R.M. Iyer, J. Chem. Soc., Faraday Trans. 89 (1993) 1143.
[34] K.I. Hadjiivanov, M.M. Kantcheva, D.G. Klissurski, J. Chem. Soc., Faraday Trans. 92 (1996) 4595.
[35] V.M. Rakic, R.V. Hercigonja, V.T. Dondur, Microporous Mesoporous Mater. 27 (1999) 27.
[36] K.I. Hadjiivanov, L. Dimitrov, Microporous Mesoporous Mater. 27 (1999) 49.